

Rothamsted Repository Download

A - Papers appearing in refereed journals

Blanchy, G., Watts, C. W., Ashton, R. W., Webster, C. P., Hawkesford, M. J., Whalley, W. R. and Binley, A. 2020. Accounting for heterogeneity in the \square – \square relationship: Application to wheat phenotyping using EMI. *Vadose Zone Journal*. 19 (article), p. e20037.
<https://doi.org/10.1002/vzj2.20037>

The publisher's version can be accessed at:

- <https://doi.org/10.1002/vzj2.20037>

The output can be accessed at:

<https://repository.rothamsted.ac.uk/item/9839z/accounting-for-heterogeneity-in-the-relationship-application-to-wheat-phenotyping-using-emi>.

© 21 May 2020, Please contact library@rothamsted.ac.uk for copyright queries.

Accounting for heterogeneity in the θ – σ relationship: Application to wheat phenotyping using EMI

Guillaume Blanchy¹  | Christopher W. Watts²  | Rhys W. Ashton² | Colin P. Webster² | Malcolm J. Hawkesford² | William R. Whalley² | Andrew Binley¹

¹Lancaster Univ., Lancaster, Lancashire LA1 4YW, UK

²Rothamsted Research, Harpenden, Hertfordshire, AL5 2JQ, UK

Correspondence

Guillaume Blanchy, Lancaster Univ., Lancaster, Lancashire LA1 4YW, UK.
Email: g.blanchy@lancaster.ac.uk

Funding information

Biotechnology and Biological Sciences Research Council, Grant/Award Number: BB/P016855/1

Abstract

Geophysical methods, such as electromagnetic induction (EMI), can be effective for monitoring changes in soil moisture at the field scale, particularly in agricultural applications. The electrical conductivity (σ) inferred from EMI needs to be converted to soil moisture content (θ) using an appropriate relationship. Typically, a single global relationship is applied to an entire agricultural field; however, soil heterogeneity at the field scale may limit the effectiveness of such an approach. One application area that may suffer from such an effect is crop phenotyping. Selecting crop varieties based on their root traits is important for crop breeding and maximizing yield. Hence, high-throughput tools for phenotyping the root system architecture and activity at the field scale are needed. Water uptake is a major root activity and, under appropriate conditions, can be approximated by measuring changes in soil moisture from time-lapse geophysical surveys. We examine here the effect of heterogeneity in the θ – σ relationship using a crop phenotyping study for illustration. In this study, the θ – σ relationship was found to vary substantially across a field site. To account for this, we propose a range of local (plot specific) θ – σ models. We show that the large number of parameters required for these models can be estimated from baseline σ and θ measurements. Finally, we compare the use of global (field scale) and local (plot scale) models with respect to ranking varieties based on the estimated soil moisture content change.

1 | INTRODUCTION

Over the past two decades, there has been a growth in the use of geophysical methods in agriculture (Allred, Daniels, & Ehsani, 2008). This has been driven, in part, by the need to assess variation in soil properties in a noninvasive manner over relatively large scales. Geophysical methods in such a context are a subset of proximal soil sensing approaches

(Viscarra Rossel, Adamchuk, Sudduth, McKenzie, & Lobsey, 2011). Measurements of properties, such as electrical conductivity, are typically treated as a proxy for a soil property or state of interest (e.g., soil texture, bulk density, or soil moisture content). Such methods may also be used in a time-lapse manner to examine changes in soil properties or states (e.g., changes in texture or soil density due to land management practices). Typically, maps of a geophysical property are presented in a qualitative manner. Although this can be effective in some cases, the ability to estimate quantitatively the property, or state, of interest offers greater scope for a wider range of agricultural applications. To achieve such

Abbreviations: EMI, electromagnetic induction; ERT, electrical resistivity tomography; HCP, horizontal coplanar mode; Rx, receiver; Tx, transmitter; VCP, vertical coplanar mode.

This is an open access article under the terms of the Creative Commons Attribution License, which permits use, distribution and reproduction in any medium, provided the original work is properly cited.

© 2020 The Authors. *Vadose Zone Journal* published by Wiley Periodicals, Inc. on behalf of Soil Science Society of America

quantification, the relationship between the geophysical proxy and the soil property or state is required. Such relationships may be spatially variable, particularly over field scales typical in agricultural studies. Here, we assess such heterogeneity in a wheat (*Triticum aestivum* L.) phenotyping study and propose practical methods to account for such variability.

1.1 | Field-scale phenotyping bottleneck

Wheat is one of the main staple crops in the world. It has been bred over centuries for specific traits, most of which are aboveground characteristics. Given uncertain future climatic conditions, there are demands for more resilient breeds. A key component of such resilience lies in the root system of the crop. Deeper root systems are correlated with higher yield and higher resistance to drought (Wasson et al., 2012). Usually the root system of a crop is assessed in the laboratory or in the greenhouse. However, field studies of the root system are essential to understand more about how each variety adapts to its environment. The typical approach of assessing the root system of a crop in the field is by direct sampling (Wasson et al., 2014). Such methods are destructive, labor-intensive, and expensive in a conventional breeding program with a large number of breeding lines. An alternative, less invasive, and quicker approach is to consider the root activity rather than the quantity of roots. Such methods rely on observing changes in soil moisture to infer root activity (Beff, Günther, Vandoorne, Couvreur, & Javaux, 2013; Garré et al., 2013; Michot et al., 2003; Srayeddin & Doussan, 2009). Different methods to measure efficiently this change in soil moisture were explored by Whalley et al. (2017) for different wheat genotypes. Among them, geophysical methods, such as electrical resistivity tomography (ERT) and electromagnetic induction (EMI) appear promising as a means of measuring a proxy to observe the dynamics of soil moisture of the subsurface (Binley et al., 2015). Shanahan, Binley, Whalley, and Watts (2015) illustrate the use of EMI for differentiating soil drying from different wheat genotypes in a phenotyping context. In their study, the relationship between the observed proxy (soil apparent electrical conductivity) and soil moisture content was assumed to be homogeneous across the study site. Huang, Purushothaman, McBratney, and Bramley (2018) also use EMI as a proxy for plot-scale crop water of different chickpea (*Cicer arietinum* L.) genotypes. Other examples of the use of EMI in crop-related studies include Cassiani et al. (2012), von Hebel et al. (2014), and Moghadas, Jadoon, and McCabe (2017).

1.2 | Electromagnetic induction

The EMI method measures the soil apparent electrical conductivity (σ_a) in a noncontact or invasive manner. A standard

Core Ideas

- Field-scale relationships between θ and electrical conductivity can be inappropriate.
- Pedophysical parameters can, in some cases, be approximated using baseline data.
- The method is illustrated for application of EMI mapping for phenotyping wheat crops.

EMI device is composed of a transmitter (Tx) coil and at least one receiver (Rx) coil. The transmitter coil generates a transient electromagnetic field. This primary field induces eddy currents in the ground; the magnitude of eddy currents generated is a function of the soil electrical conductivity, σ . The eddy currents then induce a secondary electromagnetic field. Both primary and secondary electromagnetic fields are measured by the receiver coils. The out-of-phase component of their complex ratio is used to compute the apparent electrical conductivity (σ_a) of the subsurface. Electromagnetic induction measurements can be made in vertical and horizontal coplanar orientations, with different depth-sensitivity functions. Several current instruments, such as the one used in this study (Mini-Explorer from GF-Instruments), have multiple receiver coils.

The relationship between depth-specific σ and measured σ_a , for a given coil orientation, and the distance between the Tx and Rx, can be described using a simple function—the “cumulative sensitivity function” (McNeill, 1980). A more accurate, but more complex, method based on Maxwell’s equations (Andrade, Fischer, & Valenta, 2016; von Hebel et al., 2014) can also be used to describe such a relationship. Using measurements made on a multi-coil device, depth-specific σ can be determined from inverse modelling of the σ – σ_a relationship. The inversion process seeks the best distribution of depth-specific σ that is consistent with all observed σ_a values for different coil spacings and orientations. A prerequisite, considered by some authors, for inversion is that the apparent values given by the different EMI configurations need to be calibrated with results from an ERT survey (Lavoué et al., 2010). More details about EMI inversion can be found in von Hebel et al. (2014).

Electromagnetic induction measurements have been extensively used to map field heterogeneities and produce detailed soil maps for the definition of management zones in precision agriculture (Brevik, Fenton, & Lazari, 2006; Corwin & Lesch, 2003; King et al., 2005). More recently, multi-coil EMI instruments have provided greater depth-specific information in agricultural studies, allowing assessments of depth-specific σ and its link to aboveground crop performance indicators (Brogi et al., 2019; von Hebel et al., 2018).

1.3 | Soil moisture content–electrical conductivity relationships

The soil electrical conductivity is controlled by a number of properties (soil texture, organic matter content) and states (soil temperature, pore water electrical conductivity, bulk density, and soil moisture content). The soil structural state and its properties control σ through pore connectivity and porosity. Such properties are also inherently linked to soil moisture content (e.g., determining residual moisture content), which has a major effect on soil σ . Temperature effects can be accounted for given local vertical soil temperature profiles, which we assume to not vary spatially inside the same field, although effects of daily or seasonal variation in temperature may need to be accounted for. The electrical conductivity of the pore water also contributes to the soil σ . In temperate climates, the variation of the pore water electrical conductivity should be minimal in rain-fed settings. However, this has a greater impact in irrigated conditions, as the irrigated water (e.g., groundwater sourced) is likely to have a different ionic composition and temperature than the pore water in the surface layers of soil. In semiarid environments, pore water conductivity effects may be significant due to enhanced salinity arising from high evaporative fluxes (Corwin & Lesch, 2005). Note that even in rain-fed environments, increase in pore-water electrical conductivity can occur due to fertilizer application.

Archie's law (Archie, 1942), developed for oil reservoir investigations, is a commonly used empirically derived model that relates the soil condition to the bulk σ . Waxman and Smits (1968) extended Archie's law by accounting for the effect of clay minerals (forming surface electrical conductivity). Several other approaches have been developed specifically for soils (Rhoades, Raats, & Prather, 1976). Laloy, Javaux, Vanclooster, Roisin, and Biielders (2011) compared a range of models for soil electrical conductivity, adopting the term "pedo-electrical" model to differentiate this from classical petrophysical approaches.

Following Laloy et al. (2011), the relationship between σ and soil moisture content (θ) can be expressed as

$$\sigma = a\theta^n + b \quad (1)$$

where a , b , and n are empirical parameters that depend on soil properties. Following Garré, Javaux, Vanderborght, Pagès, and Vereecken (2011), a is influenced by the pore water conductivity, soil texture, and porosity; b is influenced by the soil surface conductivity; and n is controlled by the soil texture. When the exponent n is close to 1, Equation 1 can be approximated by a linear relationship.

The parameters of Equation 1 may be obtained from laboratory measurements on field samples (Shanahan et al., 2015) or directly in the field, for example using a trench and soil

moisture sensors (Beff et al., 2013; Garré et al., 2013; Michot et al., 2003). Both methods provide information on a relatively small volume that might not be representative of the entire field. Indeed, from field-scale observations, the different soil textural properties also affect the θ – σ relationships, either when using σ_a (Stanley, Lamb, Falzon, & Schneider, 2014) or with depth-specific σ (Jayawickreme, Van Dam, & Hyndman, 2010). Equation 1 is usually appropriate when the soil moisture change is large and the soil heterogeneity is small. However, if significant soil heterogeneity exists, the variation in the parameters in Equation 1 may need to be accounted for. This effect may be particularly important in phenotyping studies (the determination of specific traits of crop varieties), since the differences in soil moisture change between crop lines (varieties) may be smaller compared with other studies where different species are used. Whether depth-specific or apparent values (like in this study) are considered, estimates of small changes in soil moisture are likely to be affected by heterogeneity in the θ – σ relationship (Equation 1).

Furthermore, in a phenotyping context, a better prediction of the soil moisture or change in soil moisture from EMI is important, as it can help to make the variety ranking similar to the one obtained with direct soil moisture observations. Of course, if direct soil moisture data are available, there is little value in additional geophysical proxy measurements. However, in this study, the direct measurements allow us to determine what the maximum achievable information on soil moisture content obtainable from EMI measurements might be.

Therefore, this study aims (a) to quantify the spatial heterogeneity of θ – σ relationships at the field scale, (b) to determine its impact on the phenotype ranking of wheat lines, and (c) to explore approaches to account for such effects using simplified but practical approaches. The investigation uses a dataset of σ and θ measurements collected during a winter wheat field experiment.

2 | MATERIAL AND METHODS

2.1 | Field layout

Measurements were made during the 2016–2017 growing season at the Warren Field experimental farm (Woburn, UK; 52°01'06.5" N, 0°35'29.0" W) operated by Rothamsted Research. The soil at the site is classified as a sandy clay loam (District Cambisol with 54% sand, 20% silt, and 26% clay, more details in Shanahan et al., 2015). The field was sown with winter wheat at the end of 2016 and harvested in August 2017 (Bai et al., 2019). In the experiment, 71 lines of wheat and one fallow treatment (all with three replicates) were randomly distributed in three blocks. An aerial photograph showing the field experiment and the 216 plots is shown in Figure 1. Out of the 216 plots (each 9 by 1.8 m), 12 plots (four

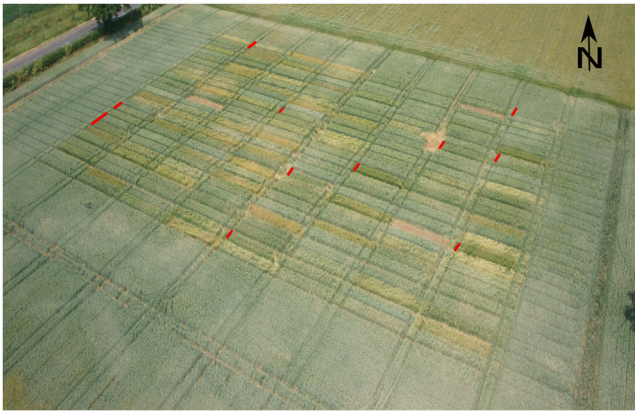


FIGURE 1 Aerial picture of the field showing the 216 plots (each 9×1.8 m) sown with winter wheat in 2016. Plots marked in red are equipped with electrical resistivity tomography (ERT) arrays

varieties) were equipped with a 24-ERT array (0.25-m spacing) placed along the middle of each plot. The ERT data were used to calibrate EMI measurements following Lavoué et al. (2010). All plots were equipped with a 1.5-m-long neutron probe access tube positioned 1 m from the edge of the plot. The ratio counts from the neutron probe were converted to soil moisture content using a field calibration ($\pm 0.01 \text{ cm}^3 \text{ cm}^{-3}$). In the field, temperature sensors recorded soil temperature at 0.1-, 0.2-, 0.3-, 0.4-, 0.6-, and 1-m depths. They were used to correct the electrical conductivity from the ERT and EMI using the ratio model (Ma, McBratney, Whelan, Minasny, & Short, 2011) with a 2% increase per degree Celsius.

2.2 | Field measurements

Three sets of EMI measurements were collected on each plot with a Mini-Explorer instrument (GF Instruments) according to the guidelines provided in Shanahan et al. (2015). They were then averaged to obtain a mean for each plot. Surveys were conducted on dates: 8 Oct. 2016, 2 Mar. 2017, 16 Mar. 2017, 3 Apr. 2017, 27 Apr. 2017, 16 May 2017, and 1 June 2017. Data from some plots were discarded because of two high voltage cables buried under the field. The filtering used the standard deviation of the three sets of EMI data for each plot.

The Mini-Explorer contains three receiver coils with separations 0.32, 0.71, and 1.18 m from the transmitter coil. Measurements in the two modes (horizontal coplanar mode [HCP] and vertical coplanar mode [VCP]) were obtained. Therefore, six measurements of apparent conductivity were made. The normalized sensitivity pattern (McNeill, 1980) of each configuration is shown in Figure 2a (note that in Figure 2a and hereafter, the notation [e.g., HCP0.32] is used to identify coil orientation and spacing [HCP with a 0.32 m coil spacing]).

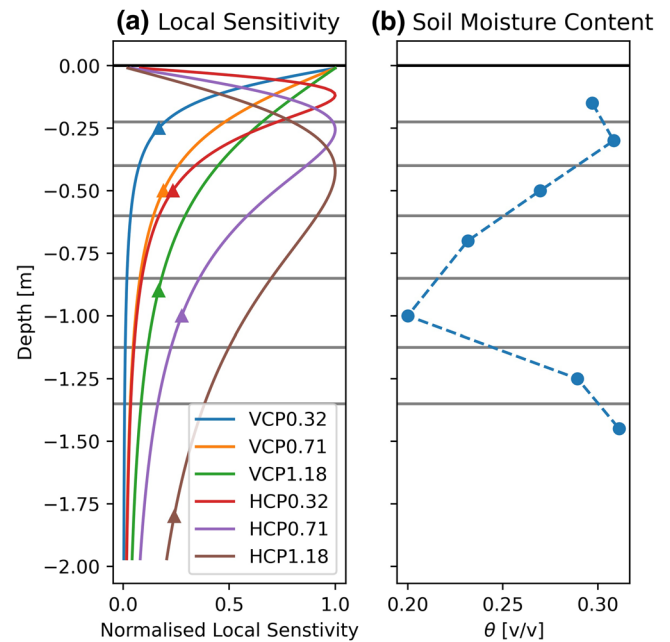


FIGURE 2 (a) Normalized local sensitivity pattern for the six pairs of coil orientations and coil separations available on the Mini-Explorer instrument. The triangles show the depth above which there is 70% cumulative sensitivity (commonly referred to as the effective depth of investigation). (b) Measured soil moisture content profile by neutron probe. To build the apparent soil moisture content, each depth-specific soil moisture content (θ) measurement is multiplied by the integrated electromagnetic induction (EMI) sensitivity corresponding to its depths (between the gray lines) and then summed (see Section 3.1). HCP, horizontal coplanar mode; VCP, vertical coplanar mode

Figure 2b shows example soil moisture data from the neutron probe taken at seven depths. For each depth, the gray lines denote the limits used to compute the local sensitivity weights used in the computation of the apparent soil moisture content (Section 3.1).

The ERT measurements were collected using a 48 Syscal Pro (Iris Instrument) on similar dates to the EMI (2 Mar. 2017, 16 Mar. 2017, 3 Apr. 2017, 27 Apr. 2017, 16 May 2017, 1 June 2017, and 23 June 2017). Neutron probe measurements were collected on 16 Mar. 2017, 5 Apr. 2017, 26 Apr. 2017, 18 May 2017, 23 June 2017. Nitrogen fertilizer (Nitram 37.5% N) was applied on 10 Apr. 2017 and 25 Apr. 2017 as pellets. Whenever possible, ERT and EMI measurements were collected on the same day. Neutron probe datasets were collected as close as possible to the ERT/EMI dataset, either on the same day or before or after an interval of a few days, thus minimizing disturbance from any rainfall events. Note that the neutron probe dataset of mid-May was taken after a large overnight rainfall event. This had an impact on the shallow measurements (0.15- and 0.30-m depths) but did not influence the deeper measurements. Note also that N fertilizer was applied just before the measurement at the end of May. However, because of its

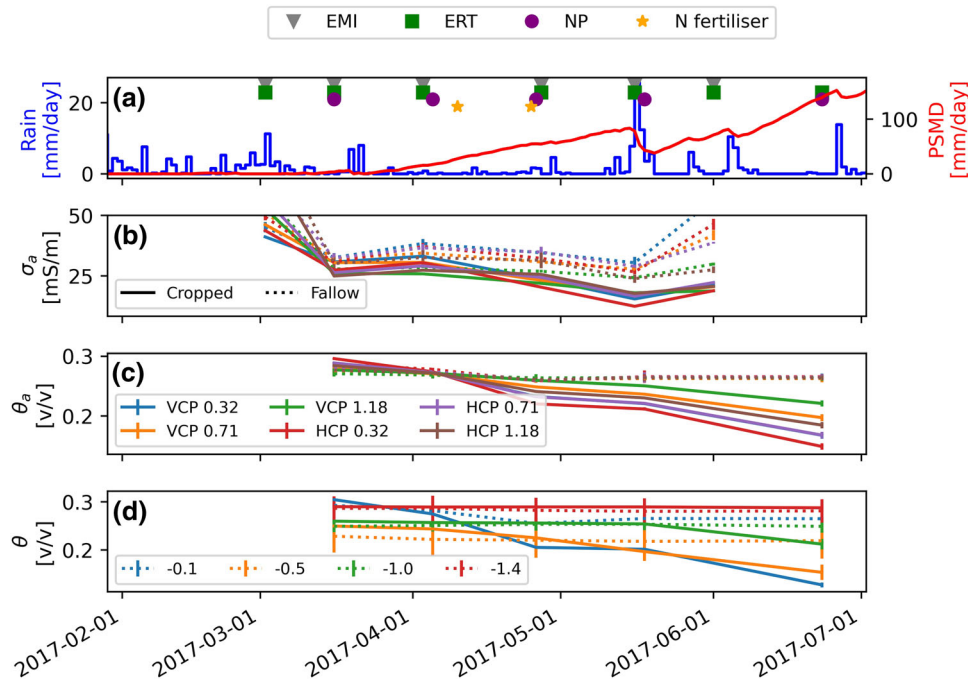


FIGURE 3 (a) Rainfall and potential soil moisture deficit (PSMD) with markers corresponding to the collection date of the electrical resistivity tomography (ERT), electromagnetic induction (EMI), and neutron probe (NP) dataset. (b) Evolution of soil apparent electrical conductivity (σ_a) from EMI. (c) Evolution of computed apparent soil moisture content (θ_a). (d) Evolution of the measured soil moisture content from neutron probe for selected depths. Error bars are SEM (sometimes too small to be visible on the graph). Dotted lines are averages of the fallow plots, whereas solid lines are averages of the cropped plots. HCP, horizontal coplanar mode; VCP, vertical coplanar mode

application as dry pellets and the lack of large rainfall events, it is unlikely that it had fully dissolved into the soil at the time of the end of May survey. This could have caused a significant increase in the pore water electrical conductivity, and hence in our EMI and ERT measurement, no sharp increase in observed electrical conductivity is apparent. At the end of the field campaign, four different datasets of ERT, EMI, and neutron probe measurements were available to derive pedo-physical relationship for each plot. Despite the limited number of time-lapse data collected on the same plot, the larger number of plots screened enables us to capture well the temporal and spatial variability across the field.

3 | RESULTS

3.1 | Apparent soil moisture content

To allow comparison with observed apparent conductivity measurements and to avoid any inversion artifacts that can arise from EMI inversion, an “apparent” soil moisture was computed based on the weights of the EMI cumulative sensitivity function (Figure 2a) following the approach given by Martini et al. (2017). The θ measurements of a given profile (Figure 2b) were multiplied by their respective depth-specific normalized local sensitivity and then summed to obtain an apparent soil moisture content (θ_a). The shape of the normal-

ized sensitivity function is determined by the same parameters as for the EMI: the coil orientation (HCP or VCP) and the coil spacing (0.32, 0.71, or 1.18 m). Thus, for each pair of coil orientation and coil spacing, a different θ_a was obtained, for comparison with the observed σ_a from EMI. The apparent soil moisture content θ_a is given by

$$\theta_a = \sum_i^n \theta_i s_i \quad (2)$$

where θ_i is the measured soil moisture content of layer i , and s_i is the sensitivity of the layer i derived by integrating the cumulative sensitivity function between the top and the bottom depths of the layer (Figure 2). Note that the sum of s_i for the profile is equal to 1. n is the number of layers.

3.2 | Evolution

Figure 3a shows the different collection times as well as selected weather data during the experiment. Figures 3b, 3c, and 3d show the evolution of the different observed and computed belowground variables. Note the clear difference between the averages of the fallow and cropped plots, demonstrating a substantial effect of the crop in the soil moisture changes over time (i.e., crop water uptake accounts for a substantial change in soil moisture). Note that the σ_a from EMI shows a peak around 1 Mar. 2017 and 1 June 2017. This can be

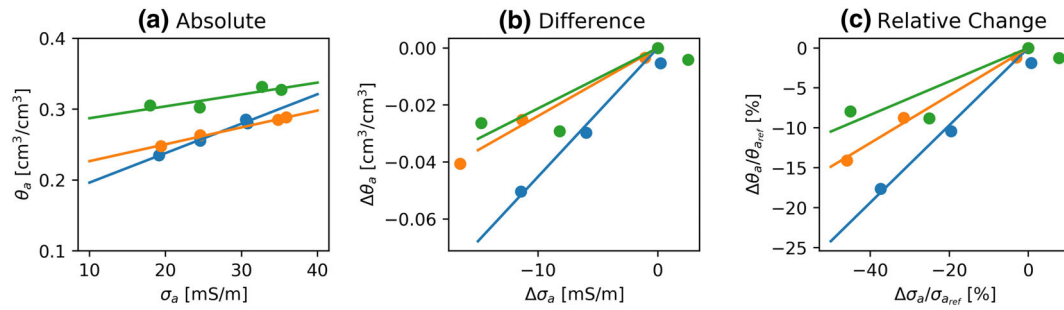


FIGURE 4 Soil moisture content (θ)–electrical conductivity (σ) relationships between apparent θ and σ (θ_a and σ_a) collected in the field in three example plots with the same variety expressed as: (a) absolute, (b) difference, and (c) relative change. $\sigma_{a,ref}$ is the baseline apparent electrical conductivity and $\theta_{a,ref}$ is the baseline apparent soil moisture content from which the changes are computed. Data for each plot are differentiated by a different color symbol or line

explained by the large amount of rainfall on the previous day. Note that no soil moisture content data were collected on 1 June 2017, hence the series does not show a similar increase. The analysis uses the data from the four following dates for which EMI, ERT, and neutron probe measurements were all available: 16 Mar. 2017, 5 Apr. 2017, 26 Apr. 2017, and 18 May 2017.

3.3 | Time-lapse approach

Time-lapse monitoring of σ allows the removal of stationary effects of the soil (soil organic matter, soil texture) on the θ – σ relationship (Robinson, Abdu, Lebron, & Jones, 2012; Shanahan et al., 2015). This approach relies on the measurements of a baseline (in this case, where no crop effect is present), which is usually made at the beginning of the growth season when the field is at or near field capacity. All subsequent surveys can be compared with this baseline, consequently revealing the main drying pattern mainly driven by root activity. For the experiment presented here, the baseline data were measured on 16 Mar. 2017.

There are two ways to compute changes from the baseline conditions: (a) by computing the *difference*, or (b) by computing the *relative change*. Assuming a linear relationship between θ and σ ($n = 1$ in Equation 1), the equations below can be written.

The difference is simply the difference between σ and σ_{ref} :

$$\Delta\sigma = \sigma - \sigma_{ref} = (a\theta + b) - (a\theta_{ref} + b) = a\Delta\theta \quad (3)$$

where σ_{ref} and θ_{ref} are the baseline σ and θ , respectively.

The relative change is the difference between σ_1 and σ_{ref} normalized by the baseline σ_{ref} (Equation 4). It is given by

$$\frac{\Delta\sigma}{\sigma_{ref}} = \frac{a\Delta\theta}{a\theta_{ref} + b} \quad (4)$$

Computing differences (Equation 3) removes the effect of “offset” b but retains “slope” a , which may vary across the site. In contrast, working with relative change (Equation 4) retains the effects of a and b , unless b is relatively small. In the latter case, Equation 4 can clearly be simplified to link directly the relative change in σ with the relative change in θ as

$$\frac{\Delta\sigma}{\sigma_{ref}} = \frac{\Delta\theta}{\theta_{ref}} \quad (5)$$

The expressions above were used to explore ways in which the variation of a and b within a site can be accounted for.

3.4 | Observations

Figure 4 shows the different relationships between σ_a and θ_a for three plots with the same variety in the field site. The variation between the three responses (expressed as absolute, difference, or relative change) reveals the effect of spatial variability across the site, highlighting the limitation of adopting a single global relationship.

Figure 5 shows the distribution of θ_a and σ_a in April 2017 and their difference with respect to the baseline in March 2017 (16 Mar. 2017). From Figure 5, it can be seen that the patterns for both absolute and differences are different. This illustrates the effect of different θ – σ relationships observed in Figure 4. Both patterns in σ_a and θ_a values remain consistent for the different collection dates.

3.5 | Development of local model

Typically, a few samples from the field are collected to build a *global* unique relationship between θ and σ . We can express this relationship as

$$\sigma = a_g\theta + b_g \quad (6)$$

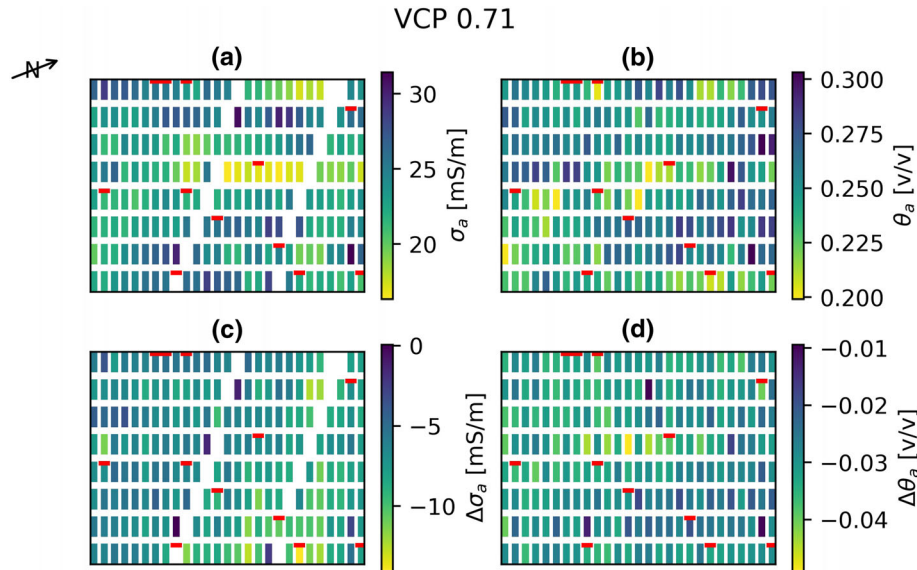


FIGURE 5 General schematic layout of the random block experiment (not to scale) on 17 Apr. 2017. One rectangle represents one 9-m by 1.8-m plot. Plots marked with a red line were equipped with an electrical resistivity tomography (ERT) array. The soil apparent electrical conductivity (σ_a) value for each plot is the average of three replicates. (a) Shows the distribution of σ_a (VCP0.71 with an effective depth of 0.5 m). (b) Shows the corresponding apparent soil moisture content (θ_a) from neutron probe measurements. (c, d) Difference in σ_a and θ_a , respectively, from the baseline measurement of 16 Mar. 2017. Spatial heterogeneity exists in both variables and even in their differences. Blank plots in the electromagnetic induction (EMI) maps are plots affected by buried high-voltage cables. VCP, vertical coplanar mode

$$\Delta\sigma = a_g \Delta\theta \quad (7)$$

where the global a_g and b_g parameters are identical for all the plots.

However, for a heterogeneous field, using this global relationship may lead to substantial errors in the estimation of soil moisture content changes. In order to overcome this, we explored *local* models allowing the assignment of a unique θ – σ relationship for each plot:

M1. *Linear local* model, based on Equation 1 assuming $n = 1$. This model has two plot-specific parameters: i is the plot number, the slope is a_i , and the offset is b_i :

$$\sigma = a_i \theta + b_i \quad (8)$$

Figure 6 illustrates, using all measurements, how well the linear global model and linear local model (M1) perform. There is a clear (and expected) improvement of the prediction of soil moisture content with the linear local model. Note that an exponential model (not shown here) following Equation 1 was also fitted and has similar performance to the linear model ($R^2 = .37$ for the global exponential model; $R^2 = .82$ for the local exponential model). Consequently, the linear model is adopted hereafter.

As seen in Figure 6, the local linear model outperforms the global linear model but increases the number of parameters needed. More importantly, a full set of monitored soil moisture content values is needed, making the geophysical proxy

approach redundant. As a first step to reduce the number of local parameters, we introduce two new models:

M2. *Multi-offsets* model: a linear model where each plot has its own offset b_i but share a common slope a_g :

$$\sigma = a_g \theta + b_i \quad (9)$$

M3. *Multi-slopes* model: this model only applies to differences in values and is based on Equation 3, with each plot having its own slope a_i . This model has one parameter per plot (slope):

$$\Delta\sigma = a_i \Delta\theta \quad (10)$$

Mathematically, the multi-offsets model (M2) produces a set of parallel σ – θ relationships similar to Figure 4a, whereas the multi-slopes model leads to a set of conical $\Delta\sigma$ – $\Delta\theta$ relationships similar to Figure 4b. Both use fewer parameters than the local linear model (M1). The rationale for these simpler models is the need to reduce the number of parameters needed and increase our ability to predict them using a set of baseline measurements.

3.6 | Development of predicted local (ploal) models

All local models (M1–M3) require large amount of information for each plot and have limited practical use in a field

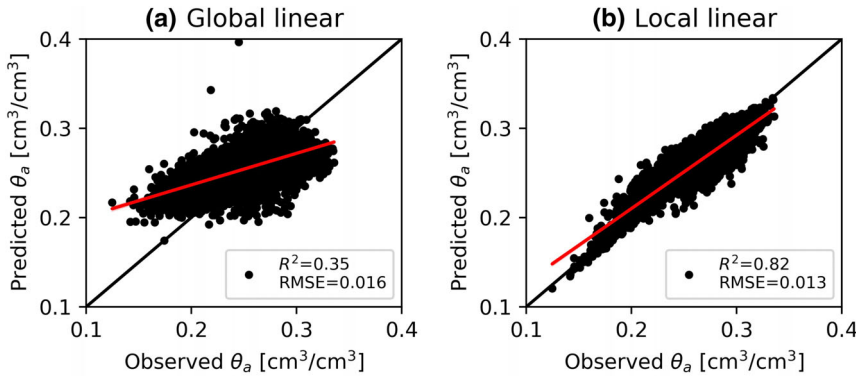


FIGURE 6 Both graphs show the observed apparent soil moisture content (θ_a) vs. the predicted θ_a from (a) the global linear model (Equation 6) and (b) the local linear model (Equation 8)

phenotyping application. As stated above, if direct measurements of soil water were available in a field experiment, there would be no benefit or value in using alternative geophysical proxy measurements. However, they allow us to determine what the maximum achievable information on soil moisture content obtainable from EMI measurements might be. As a more practical solution, we explore a range of alternative approaches where the local θ - σ relationship is known for a subset of plots and the geophysical data are used to predict those local relationships for the other plots (*plocal*).

3.6.1 | Predictors of the local parameters

The first step in developing predicted local (*plocal*) models is to identify the best estimates of the local parameters among baseline measurements. Figure 7 shows the relation-

ship between the different local parameters from each model (M1–M3) and the baseline σ_a and θ_a . It can be observed for the linear local model (M1) that the local offsets (b_i) are well related to baseline θ_a^{ref} and that the slopes (a_i) are more related to σ_a^{ref} . The multi-offsets (M2) and multi-slopes (M3) models aim to amplify those trends by reducing the number of local parameters. Using multiple local offsets but a global slope (Equation 9), the multi-offsets model (M2) displays a stronger relationship with the baseline θ_a^{ref} ($R^2 = .86$) than the linear model ($R^2 = .40$). Using multiple local slopes and no offsets (Equation 10), the multi-slopes model (M3) displays a stronger relationship with the baseline σ_a^{ref} ($R^2 = .33$) than the linear model ($R^2 = .27$).

Figure 7 allows the identification of the best predictor for each local parameter. Given local parameters from a subset of plots, a linear relationship between them and their best predictor is derived and used to predict the value of the local

VCP 0.71

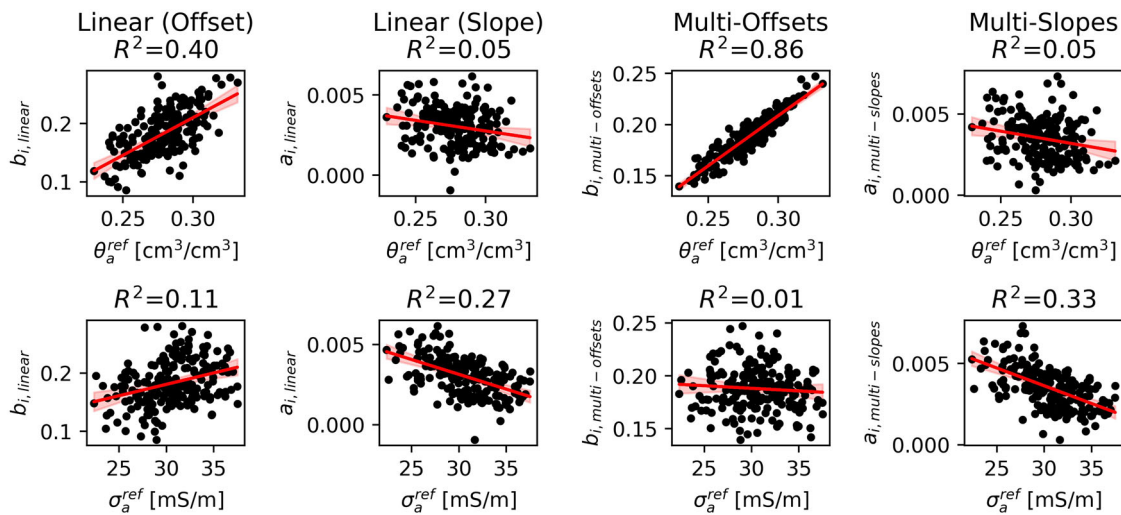


FIGURE 7 Relationships between the local parameters of the three local models (M1–M3) and the two baseline apparent electrical conductivity (σ_a^{ref}) and baseline apparent soil moisture content (θ_a^{ref}) for VCP0.71. The first two columns on the left shows the local offsets b_i and the local slopes a_i of the local linear model (M1) against the baseline measurements. The third column shows the local offsets b_i of multi-offsets model and the fourth column shows the local slopes a_i of the multi-slopes model against the baseline measurements. The red line is the line of best fit with its 95% confidence interval (red shaded region). VCP, vertical coplanar mode

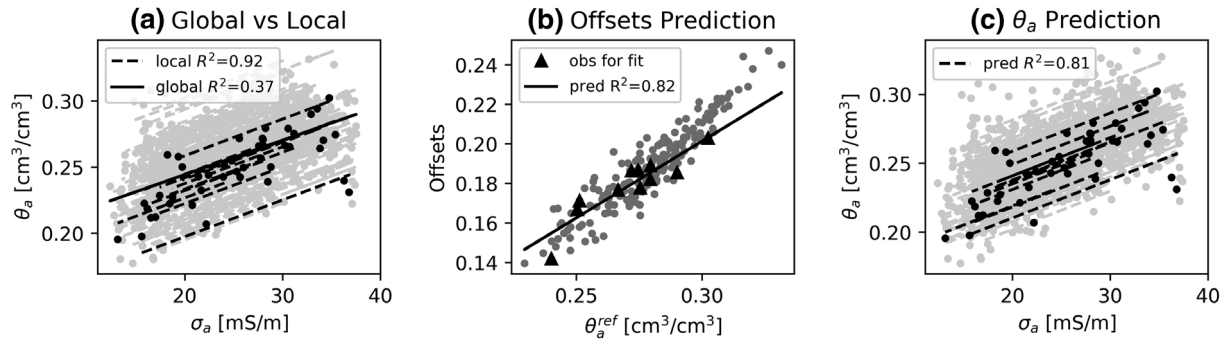


FIGURE 8 Multi-offsets model fitted with apparent values (VCP0.71). The gray dots show all the data available on the 216 plots. They represent the maximum number of information achievable if both electrical conductivity (σ) and soil moisture content (θ) are monitored on all the plots. In a more practical situation, only a subset of plots (black dots) are monitored for both σ and θ . Subplot a shows the relationship fitted with the multi-offsets model (local) as well as a global linear model, both fitted on the 216 plots. Subplot b shows the local offsets b_i vs. the baseline apparent soil moisture content (θ_a^{ref}). The black line corresponds to a linear relationship fitted on the subset of plots. This relationship is used to predict the offsets for all the other plots. Subplot c shows the multi-offsets model using the predicted offsets (plocal) from Subplot b. In Subplots a and b, the black dots and dashed lines are used to illustrate the behavior of some plots as plotting all lines will make the graph unreadable. VCP, vertical coplanar mode

parameters for the other plots. Those predicted local parameters are then used in one of the models (M1–M3). This process and the results are shown below for the multi-offsets (M2) and the multi-slopes (M3) models (M1 not shown). Hereafter, the subset of plots is composed of the 12 plots equipped with an ERT array as they are randomly distributed in the field. The choice of plots is somewhat arbitrary: another set of plots could have been selected, but they should span the largest possible range of σ and θ observed in the field.

3.6.2 | Multi-offsets model

The multi-offsets (M2) model incorporates a local offset, b_i , but a global slope, a_g (Equation 9). As an illustration, Figure 8a compares, for a subset of plots (black line and dots), the multi-offsets model with its corresponding global model for VCP0.71. The global model compared here corresponds to Equation 6 where both slope, a_g , and offset, b_g , are uniform across the field. The multi-offsets model improves the accuracy of the predicted θ_a compared with the global model ($R^2 = .92$ vs. $.37$) due to the inclusion of the local parameters b_i (Figure 8a). Both models are fitted on all the plots available. In order to decrease the amount of data needed to obtain these local offsets, a linear relationship between the local offsets b_i and the baseline θ_a^{ref} is derived using the data from a subset of plots (Figure 8b). This b_i – θ_a^{ref} relationship is then used to predict b_i for all the plots. Finally, in Figure 8c, those predicted offsets are used in the plocal multi-offsets model to obtain θ_a . In this case, the R^2 of the multi-offsets model with the predicted parameters ($.81$) is better than for the global fit ($.37$).

The multi-offsets model focuses on the absolute values and not the differences. For the latter, the multi-slopes model is adapted further.

3.6.3 | Multi-slopes model

The multi-slopes model (M3) presented in Figure 9 tries to fit a local model $\Delta\sigma_a$ and $\Delta\theta_a$ (Equation 10). Figure 9a shows a comparison of the multi-slopes model and its global equivalent. In this case the global model contains a unique slope for the whole field. Similar to Figure 8, the introduction of a local parameter (slope a_i) improves the strength of the relationship from $R^2 .71$ to $.86$. In Figure 9b, a linear relationship is derived between the local slopes a_i and the baseline σ_a^{ref} based on a subset of plots ($R^2 = .64$). This a_i – σ_a^{ref} relationship is then used to predict the values of a_i for all the other plots. Finally, those predicted slopes are used in Figure 9c in the multi-slopes model to predict $\Delta\theta_a$ for all plots. The multi-slopes model with the predicted local parameters (plocal) has a higher R^2 ($.68$) than the global fit ($.71$).

3.7 | Quality of the predicted local models

Figure 10 shows the quality of the prediction of M1, M2, and M3 using the predicted local parameters (plocal). The multi-offsets (M2) and multi-slopes (M3) models, which only have one local parameter, show better R^2 (M1: $.16$, M2: $.53$, and M3: $.60$) and a lower RMSE (M1: 0.04 , M2: 0.02 , and M3: 0.02) than the plocal linear model (M1), which has two local parameters. That means that the predicted soil moisture

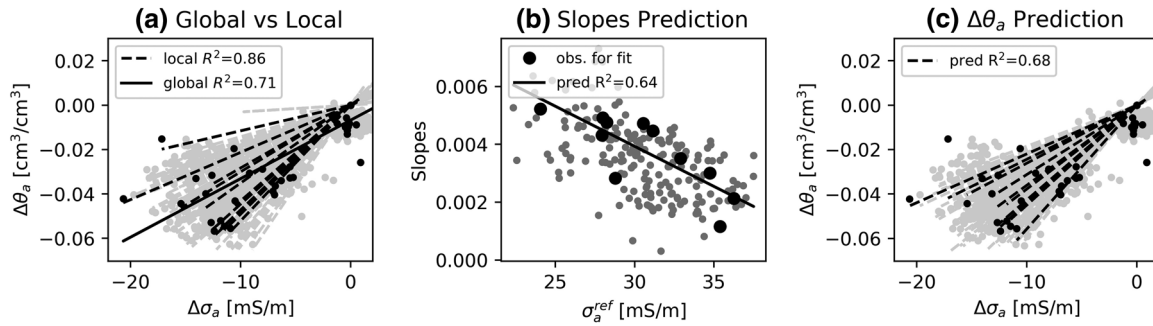


FIGURE 9 Multi-slopes model fitted with differences in apparent values (VCP0.71). The gray dots show all the data available on the 216 plots. They represent the maximum number of information achievable if both electrical conductivity (σ) and soil moisture content (θ) are monitored on all the plots. In a more practical situation, only a subset of plots (black dots) are monitored for both σ and θ . Subplot a shows the multi-slopes model as well as a global relationship with a unique slope for all 216 plots (global). Subplot b shows the local slopes according to the baseline apparent soil electrical conductivity (σ_a^{ref}). The black line corresponds to a linear relationship fitted on a subset of plots. This relationship is used to predict the local slopes for all the other plots. Subplot c shows the multi-slopes model using the predicted slopes from Subplot b (plocal). In Subplot a and b, the black dots and dashed lines are used to illustrate the behavior of some plots, as plotting all lines will make the graph unreadable. VCP, vertical coplanar mode

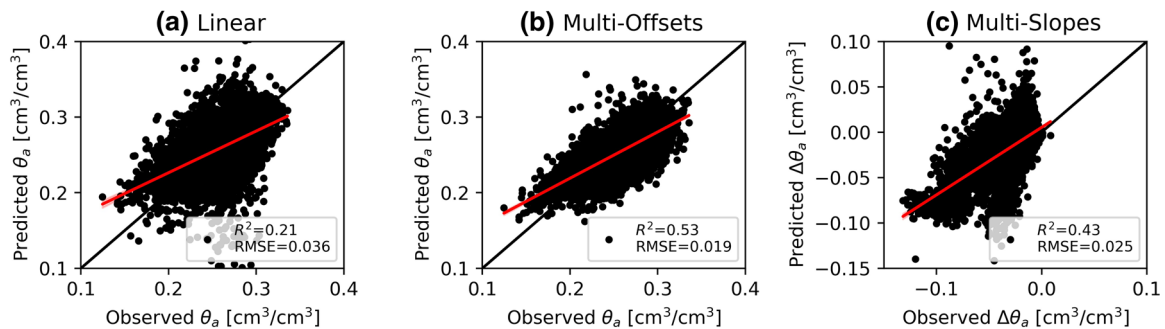


FIGURE 10 Quality of the predicted apparent soil moisture content (θ_a) vs. the observed θ_a from (a) linear, (b) multi-offsets, and (c) multi-slopes models with predicted local parameters. The red line is the line of best fit with its 95% confidence interval (red shaded region). Both multi-offsets and multi-slopes models have one local parameter, whereas the linear model has two

content from the multi-offsets (M2) or multi-slopes (M3) models is more accurate than from the linear model (M1).

3.8 | Choice of the size of the subset of plots for plocal models

The size of the subset of plots needed for the plocal models needs to be chosen carefully. Figure 11 shows the effect of the number of selected plots on the RMSE of the prediction for the multi-offsets (M2) and the multi-slopes (M3) models. In this case, the RMSE does not change much if >10 plots are included in the subset.

3.9 | Effect on the variety ranking

In a phenotyping context, we expect similarity in the rank of varieties whether observed (from neutron probe) or predicted

(from EMI) soil moisture values are used. To assess the ranking improvement the predicted values of the global, local, and plocal models are averaged by variety. Then, the Spearman's rank correlation is computed between the observed and the predicted θ_a (or $\Delta\theta_a$). The Spearman's rank correlation has the advantage of being directly related to the ranking of the variety, which is a commonly used metric in crop breeding. A high value for this coefficient means, in our case, that higher predicted θ_a is associated with higher observed θ_a or that larger predicted θ_a differences are associated with larger observed θ_a differences, from examining absolute values or differences, respectively.

Figure 12a shows the Spearman's rank correlations for the multi-offsets (M2) model using the baseline θ_a^{ref} as predictor of the local offsets. Figure 12b shows the Spearman's rank correlations for the multi-slopes (M3) model using the baseline σ_a^{ref} as predictor of the local slopes.

Using the data in this study, the global models offer poor correlation compared to the local models, due to the

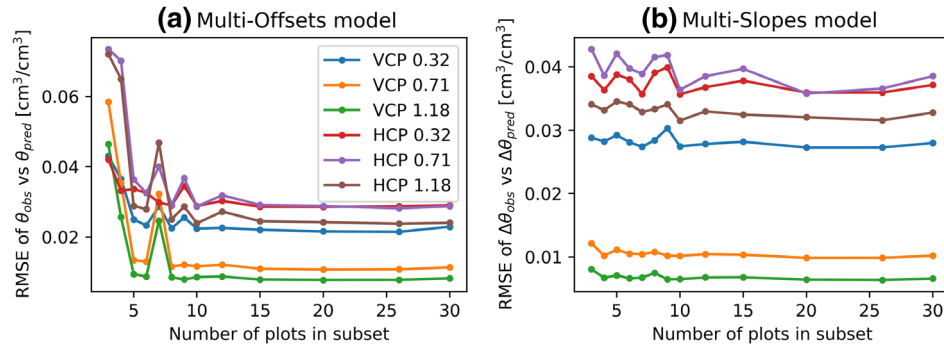


FIGURE 11 Effect of the size of the subset of plots on the predictions of the plocal (a) multi-offsets and (b) multi-slopes. After sorting the plots according to the baseline soil apparent electrical conductivity (σ_a), a subset of a given number of plots is selected at regular interval on the whole range of baseline values. θ_{obs} and θ_{pred} are observed and predicted soil moisture content. HCP, horizontal coplanar mode; VCP, vertical coplanar mode

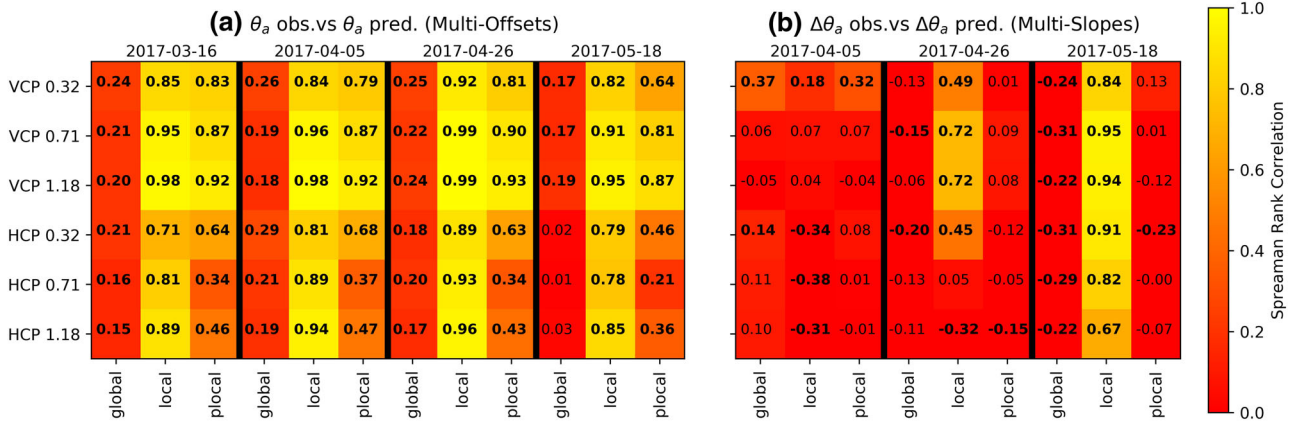


FIGURE 12 Improvement in variety ranking in terms of the Spearman’s rank correlation coefficient for (a) the multi-offsets and (b) the multi-slopes models. Each row of the table corresponds to a coil configuration. The columns are grouped by dates and subdivided into global, local and plocal models. The global models use field-specific parameters, and the local models use plot-specific parameters estimated using all the data available. The plocal model use the predicted plot-specific parameters estimated from baseline measurements (as in Figure 8b and Figure 9b). Bold numbers denote a significant correlation ($p < .05$). HCP, horizontal coplanar mode; VCP, vertical coplanar mode; θ_a , apparent soil moisture content

heterogeneity of the σ – θ relationship. This is true for all coil configurations. The plocal models (i.e., the models using the predicted local parameters) show higher correlation compared to their global equivalent. For the multi-offsets model, the improvement between global and the plocal is substantial (Figure 12a). When considering changes in soil moisture content (Figure 12b), the correlation with the global model is sometimes negative. This is a concern, as it means that an increase in σ_a can be associated with a decrease in θ_a after application of the global model. The local multi-slopes models increases this correlation substantially, especially for later dates. However, the plocal multi-slopes model shows relatively poor correlation even if it can compensate for the negative correlation observed in the global model in some cases.

4 | DISCUSSION

4.1 | Methodological limitations

The approach presented in this manuscript relies on apparent and not depth-specific electrical conductivity measurements to avoid the uncertainty arising from EMI inversion. Hence, we converted soil moisture content to apparent values using the practical cumulative sensitivity function (McNeill, 1980). However, the latter can have limitations especially on heterogeneous conductive soils. To estimate the errors that can arise from using the cumulative sensitivity function, Maxwell’s equations can be used to reconstruct sensitivity functions based on a synthetic two-layer profile comparable with what is observed in the field (Callegary, Ferré, & Groom, 2007).

Both sensitivity functions are then used to compute the apparent soil moisture content. The maximum discrepancy between the two approaches is $0.01 \text{ cm}^3 \text{ cm}^{-3}$, which is similar to the neutron probe accuracy ($0.01 \text{ cm}^3 \text{ cm}^{-3}$). Given the magnitude of the errors, this probably has a more important impact on the changes in soil moisture content than on the absolute values. This might explain why the multi-slopes model works less well than the multi-offsets model in this study.

The dynamics of the soil moisture are complex, and isolating the effect of root activity is challenging. Whenever possible, measurements were collected at increasing potential soil moisture deficit and away from significant rainfall events (Figure 3). The drying observed in cropped plots compared with fallow plots suggests a substantial effect of the root activity (Figure 3). However, the proposed approach does not aim at univocally measuring root water uptake, but rather at comparing soil moisture variation mainly induced by root activity for the different varieties.

The models described in the manuscript are simple linear models. More complex relationships can be used to relate soil moisture to electrical conductivity. For example, an exponential model was initially tested and showed similar performance to the linear model (see Section 3.5), hence the simplest model is chosen. In the linear models presented, the slope can be related to the soil surface conductivity, while the offset is more a function of the pore water conductivity. Both are functions of the soil texture and porosity (Garré et al., 2011). We do not have the information to investigate further the impact of these soil properties on the pedophysical parameters we derived for this field.

This study assumes that the samples taken on each plot (EMI, NP) are representative of the entire plot and that no substantial heterogeneity exists within the plot itself. Although we have no data to assess that this assumption is fulfilled for all the plots, the inverted ERT sections, which span 5.75 out of the 9 m of the plot length, suggest that this is the case.

One can question if the plot is the appropriate scale at which to investigate the variability of the θ - σ relationships. The use of variogram analysis can certainly help to determine the appropriate length scale at which the heterogeneity occurs. However, this method was not explored in this study, as our approach relies on the plot scale for practical reasons and to be consistent with additional phenotyping measurements at the site.

Finally, it has been assumed that the root system of the crop itself did not significantly contribute to the soil bulk apparent conductivity. Although there is evidence that suggests that coarser roots can affect the soil bulk electrical conductivity (Amato et al., 2008; Mary et al., 2017), finer herbaceous roots have been found to have a signal in magnitude similar to the effect of grain size or soil moisture content (Amato et al., 2009). Nevertheless, recent studies were able to isolate the electrical signature of roots themselves (Tsukanov

& Schwartz, 2020). This could have great potential for phenotyping applications.

4.2 | Ranking performance

Fitting a global model with field-specific parameters to all the data can lead to a satisfactory prediction of the soil moisture content, particularly if the differences expected between the treatments are large, such as for different types of vegetation (Jayawickreme et al., 2010), between fallow and cropped plots or between different soil types. However, when comparing a large number of similar varieties, this global model may be limited (Figure 12). In a phenotyping application, as here, using such a relationship may lead to false ranking of variates when using geophysical data (Figure 12). As observed by Farahani, Buchleiter, and Brodahl (2005) for nonsaline soil, higher σ_a is not always associated with greater soil moisture. Taking into account differences, it can also be seen that a large reduction in σ_a is also not always associated with a large reduction in θ_a . The negative correlations sometimes observed are of concern, as they lead to very different varieties ranking whether we consider σ_a or θ_a (Figure 12). The use of local parameters in the σ - θ relationship increases the Spearman's rank correlation for later dates as the soil moisture differences from the baseline become larger. The large number of parameters needed to fit the local models (linear, multi-offsets, or multi-slopes) can be reasonably reduced using a relationship between the local parameters and the baseline σ_a or θ_a fitted on a subset of plots. The resulting plocal models that use those predicted parameters increase the accuracy of the prediction compared with global models (Figure 10). The R^2 value is often similar to or higher than those of the corresponding global models, but the ranking assessed (using the Spearman's rank correlation) is usually better (Figure 12). Note that the R^2 achieved are all below .6, which is relatively poor compared with what could potentially be achieved with a local relationship for all the plots (Figure 6b). Indeed, this improvement is mainly limited by the quality of the relationship between the local parameters and the predictors (Figures 8b and 9b). Hence, there is a need to select plots that span a wide range of conductivities to be monitored for both σ and θ (see Section 4.4) in order to have a more robust fit that is representative of the entire field.

4.3 | Local models and parameters predictability

As seen in Figure 7, the offsets of the linear or multi-offsets models are mainly related to the baseline θ_a . There is also a slight positive trend between the baseline σ_a and the offsets of the linear model, but it is relatively weak compared with θ_a , and it completely vanishes in the multi-offsets model. The

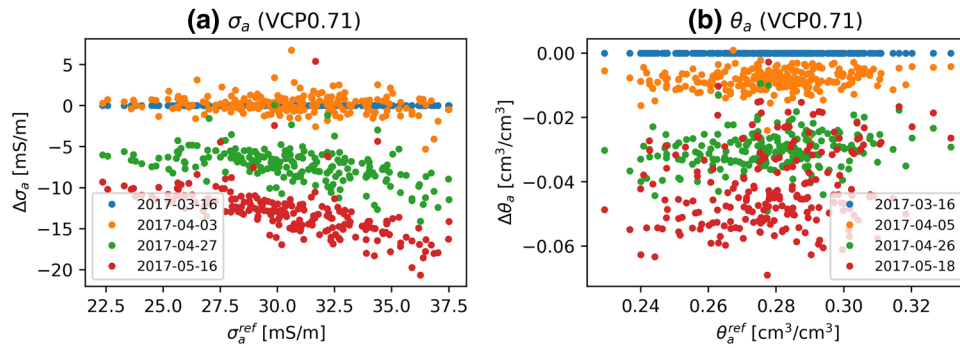


FIGURE 13 Differences in (a) soil apparent electrical conductivity (σ_a) and (b) apparent soil moisture content (θ_a) for VCP0.71 plotted against their respective baseline measurements for the different survey dates (different colors). There is larger decrease in σ_a for higher baseline soil apparent conductivity (σ_a^{ref}) in Subplot a, whereas such a downward trend cannot be seen in θ_a for larger apparent soil moisture (θ_a^{ref}) in Subplot b. VCP, vertical coplanar mode

simplification of the linear model to a multi-offsets model amplifies this dependence on the baseline θ_a . Wetter plots tend to stay wetter compared with other plots surveyed at the same time. This can be seen on Figure 4a, where each plot follows its own increasing line. This strong offset effect also explains why the relative change approach described earlier does not work well in this case. Given Equation 3, the offset is not negligible and so the equation cannot be simplified to Equation 4. That is why differences (Figure 4b) and relative changes (Figure 4c) are similar. If the offsets were negligible, Figure 4c would show a single line.

The local slopes of the local linear model are well correlated with the baseline σ_a . Considering differences, the multi-slopes model also shows good correlation between the local slopes and the baseline σ_a . The conical shape of the data shown in Figure 4b and Figure 9a for the differences illustrates how different plots have different slopes. Stanley et al. (2014) show how the slopes of the σ - θ relationships vary between two sites with contrasting textures: sites with higher clay content, for example, result in greater values than those from sandier locations.

The multi-offsets and multi-slopes models have one contrasting assumption. The former assumes a unique slope for the entire field, whereas the latter uses plot-specific slopes. Having both plot-specific offsets and slopes leads to the local linear model, but its local parameters are difficult to predict using baseline measurement (Figure 7) and hence leads to poor estimates (Figure 10). As the relationship between σ_a - θ_a is largely offset dominated, we decided to fix the slope in the multi-offsets model to reduce the number of local parameters. For the differences, the effect of the offsets disappeared (Equation 3) and only the effect of the slopes has an impact on the relationship. This leads to the multi-slopes model (Equation 10).

As seen in Figure 13, the differences in observed σ_a are well correlated with the baseline readings. Larger reductions in σ_a are seen on plots with higher baseline σ_a (Figure 13a).

Note that such a trend is not observed for θ_a (Figure 13b). The fact that the σ_a differences are still functions of the baseline reveals that the baseline σ_a contains some information on how the σ_a is likely to change: larger reductions are expected in areas of higher baseline σ_a . This behavior explains why the starting σ_a could be a good predictor of the slopes in the multi-slopes and linear models. Indeed, as the plots with higher baseline σ_a show a larger increase in σ_a with time for the same increase in θ_a , they need to have a smaller slope to compensate. Smaller slopes are then found for higher baseline σ_a (Figures 9b and 7). We believe this is related to the heterogeneity of the soil texture of the field where some areas are richer in clay than others.

Plots with higher baseline σ_a tend also to have smaller offsets as well (Figure 7), but this relationship is not strong enough to be used for parameter prediction and θ_a is preferred as the predictor (Figure 8b). Also, the prediction of the local parameters using the baseline readings is much better in the multi-offsets model (Figure 8b, $R^2 = .82$) than in the multi-slope model (Figure 9b $R^2 = .64$). This can explain why the multi-slopes model using predicted local parameters show only a slight improvement in variety ranking compared with the multi-offsets model (Figure 12).

The multi-offsets and multi-slopes models are simplified ways to account for the variability due to the spatial heterogeneity of the θ - σ relationship. By reducing the number of local parameters compared with a local linear model, the local parameters are more correlated with baseline measurements and are thus easier to predict based on a subset of plots. In that way, they increase the ranking of the varieties and the accuracy of the predicted θ_a compared with global models.

4.4 | Improvement of the time-lapse approach

A key bottleneck in using the local models (M1-M3) is the predictability of the large number of local parameters they

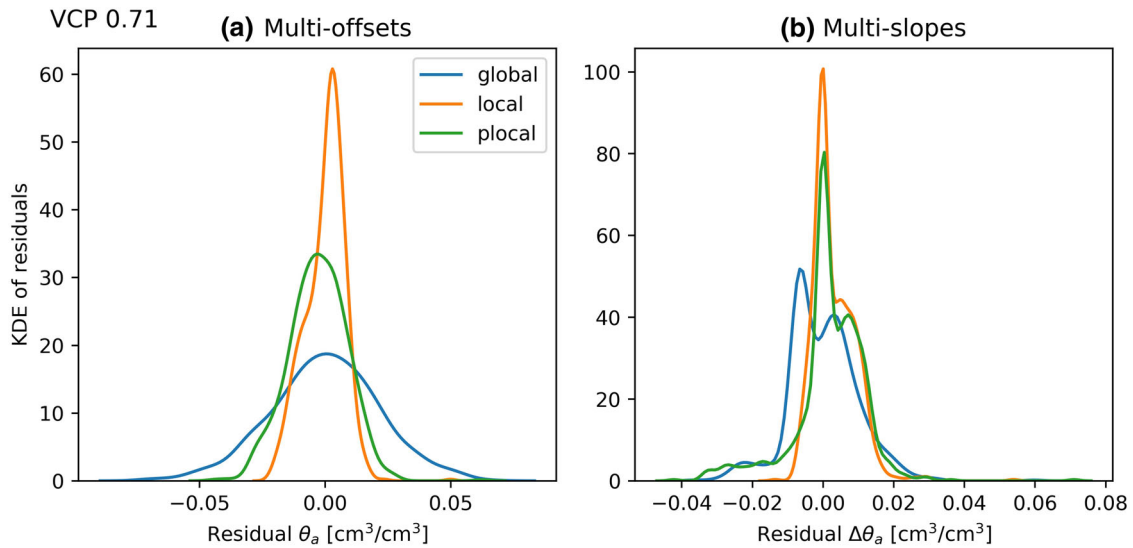


FIGURE 14 Kernel density estimate (KDE) of the residuals for the (a) multi-offsets and (b) multi-slopes models for VCP0.71. For each, the global model represent a global (field-scale) linear relationship, whereas the local models use plot-specific parameters. The plocal model is the local model with the plot-specific parameters predicted from baseline apparent soil moisture content (θ_a) or soil apparent electrical conductivity (σ_a). VCP, vertical coplanar mode

require. In this study, an approach was chosen where both variables (θ_a and σ_a) are recorded on a subset of plots. In this case, the same 12 plots that served for the ERT calibration of the EMI data were arbitrarily chosen, as they are well distributed across the field and span the whole range of observed baseline values. In our case, a sample of 12 was large enough to reach the minimum RMSE achievable (Figure 11). Given the local parameters found on the selected plots, a relationship can be derived using the baseline σ_a or θ_a . This relationship can then be used to predict the values of the local parameters for the other plots. We believe that geostatistical tools can also be used to determine the number of sampling locations. However, we have not tested these in this paper.

Considering the above, we propose an improvement to the time-lapse approach described earlier to monitor the changes in soil moisture for large crop breeding experiment. After the first baseline EMI survey, plots with contrasting σ_a are selected and equipped with soil moisture sensors (such as neutron probe access tube). The data collected on those plots will allow the estimation of the parameters for the multi-offsets and multi-slopes models. Those parameters can then be expanded to the other plots using the baseline measurements (Figure 8b and Figure 9b).

The new approach is as follows:

1. Baseline survey on all the plots to acquire σ_a^{ref} and θ_a^{ref} :
 - multi-slopes: EMI with all configurations (σ_a^{ref})
 - multi-offsets: soil moisture measurements for all depths available to build an apparent soil moisture content measurements (θ_a^{ref})

2. Selection of plots with contrasting σ_a to be equipped with θ sensors
3. Time-lapse EMI on all the plots and time-lapse θ on the selected plots: collection of multiple σ_a – θ_a datasets
4. Fit the multi-slopes (Equation 10) and multi-offsets (Equation 9) models on the selected plots to obtain the value of the local parameters: slope a_i for multi-slopes and offset b_i for multi-offset
5. Fit of linear relationship between those local parameters and the baseline value of the selected plots as in Figure 8b and Figure 9b: $a_i \sim \sigma_a^{\text{ref}}$ and $b_i \sim \theta_a^{\text{ref}}$
6. Those linear relationships are then used to predict the local parameters a_i and b_i on the other plots using their respective baseline measurements $\sigma_a^{\text{ref}}/\theta_a^{\text{ref}}$

This new approach offers a tradeoff between equipping all the plots with soil moisture sensors in order to fit a local models and using a unique global relationship for the entire field. Note that if a multi-offsets model is to be derived, baseline θ data are still needed, as they are the best predictors of the local offsets.

4.5 | Analysis of the residuals

An increase in residuals can arise due the large number of local parameters. However, as Figure 14 shows, there is no substantial increase in the distribution of those residuals for the predicted local models compared with the global and local models. We can also see from Figure 8b and Figure 9b that even if the relationship is not perfectly fitted, the predicted

parameters tend to stay in a reasonable range, avoiding the generation of outliers. Note that the residuals for the multi-slopes model are smaller than the residuals for the multi-offsets, as the range of $\Delta\theta_a$ (0 to -0.07) is smaller than the range of θ_a (0.15 to 0.35).

5 | CONCLUSIONS

High-throughput geophysical tools, in this case time-lapse EMI, offer great potential as a proxy measurement of soil moisture differences. When measurements are collected over increasing soil drying during crop growth, they may be linked to root activity in nonirrigated crop breeding field trials. The usual time-lapse approach is useful for removing the static effects of soil electrical conductivity but can be limited for ranking a large number of similar varieties in a heterogeneous environment. The spatial heterogeneity of the σ - θ relationship at the field scale has an impact on the ranking of the varieties and using a field-specific global relationship can lead to misleading interpretation. The proposed multi-offsets and multi-slopes models try to account for this heterogeneity by using plot-specific parameters that can be estimated from the baseline measurements. This improves the variety ranking between EMI and neutron probe data. A practical approach is proposed for such studies in which a baseline EMI survey is used to target sites for soil moisture monitoring, thus enhancing the ability to formulate predictions of the local σ - θ relationships. Although all the processing presented here was done with apparent conductivity measurements, the same process can be applied to depth-specific (inverted) measurements.


CONFLICT OF INTEREST

The authors declare no conflict of interest.


ACKNOWLEDGMENTS

G.B. is supported by a Lancaster University–Rothamsted Research–CEH Graduate School for Environment Ph.D. studentship. The field experiment described in the paper was funded by Syngenta, whereas the additional geophysical measurements were funded by the Lancaster University–Rothamsted Research–CEH Graduate School. M.J.H and W.R.W. at Rothamsted Research are supported by the Designing Future Wheat Programme by the UK Biotechnology and Biological Sciences Research Council (BB/P016855/1). We are grateful to associate editor Ute Wollschläger, reviewer Sarah Garré, and an anonymous reviewer for their comments on an earlier version of the manuscript.

ORCID

Guillaume Blanchy 

<https://orcid.org/0000-0001-6341-5826>

Christopher W. Watts 

<https://orcid.org/0000-0002-7223-1444>

REFERENCES

- Allred, B. J., Daniels J. J., & Ehsani M. R., editors. (2008). *Handbook of agricultural geophysics*. Boca Raton: CRC Press.
- Amato, M., Basso, B., Celano, G., Bitella, G., Morelli, G., & Rossi, R. (2008). In situ detection of tree root distribution and biomass by multi-electrode resistivity imaging. *Tree Physiology*, 28, 1441–1448. <https://doi.org/10.1093/treephys/28.10.1441>
- Amato, M., Bitella, G., Rossi, R., Gómez, J. A., Lovelli, S., & Ferreira Gomes, J. J. (2009). Multi-electrode 3D resistivity imaging of alfalfa root zone. *European Journal of Agronomy*, 31, 213–222. <https://doi.org/10.1016/j.eja.2009.08.005>
- Andrade, F. C. M., Fischer, T., & Valenta, J. (2016). Study of errors in conductivity meters using the low induction number approximation and how to overcome them. In *Proceedings of Near Surface Geoscience 2016: 22nd European Meeting of Environmental and Engineering Geophysics*. Barcelona, Spain: EAGE. <https://doi.org/10.3997/2214-4609.201602080>
- Archie, G. E. (1942) The electrical resistivity log as an aid in determining some reservoir characteristics. *Transactions of the AIME*, 146, 54–62.
- Bai, C., Ge, Y., Ashton, R. W., Evans, J., Milne, A., Hawkesford, M. J., ... Bartsch, M. (2019). The relationships between seedling root screens, root growth in the field and grain yield for wheat. *Plant and Soil*, 440, 311–326. <https://doi.org/10.1007/s11104-019-04088-9>
- Beff, L., Günther, T., Vandoorne, B., Couvreur, V., & Javaux, M. (2013). Three-dimensional monitoring of soil water content in a maize field using electrical resistivity tomography. *Hydrology and Earth System Sciences*, 17, 595–609. <https://doi.org/10.5194/hess-17-595-2013>
- Binley, A., Hubbard, S. S., Huisman, J. A., Revil, A., Robinson, D. A., Singha, K., & Slater, L. D. (2015). The emergence of hydrogeophysics for improved understanding of subsurface processes over multiple scales: The emergence of hydrogeophysics. *Water Resources Research*, 51, 3837–3866. <https://doi.org/10.1002/2015WR017016>
- Brevik, E. C., Fenton, T. E., & Lazari, A. (2006). Soil electrical conductivity as a function of soil water content and implications for soil mapping. *Precision Agriculture*, 7, 393–404. <https://doi.org/10.1007/s11119-006-9021-x>
- Broggi, C., Huisman, J. A., Pätzold, S., von Hebel, C., Weihermüller, L., Kaufmann, M. S., van der Kruk, J., & Vereecken, H. (2019). Large-scale soil mapping using multi-configuration EMI and supervised image classification. *Geoderma*, 335, 133–148. <https://doi.org/10.1016/j.geoderma.2018.08.001>
- Callegary, J. B., Ferré, T. P. A., & Groom, R. W. (2007). Vertical spatial sensitivity and exploration depth of low-induction-number electromagnetic-induction instruments. *Vadose Zone Journal*, 6, 158–167. <https://doi.org/10.2136/vzj2006.0120>
- Cassiani, G., Ursino, N., Deiana, R., Vignoli, G., Boaga, J., Rossi, M., ... Werban, U. (2012). Noninvasive monitoring of soil static characteristics and dynamic states: A Case study highlighting vegetation effects on agricultural land. *Vadose Zone Journal*, 11(3). <https://doi.org/10.2136/vzj2011.0195>
- Corwin, D. L., & Lesch, S. M. (2003). Application of soil electrical conductivity to precision agriculture: Theory, Principles, and guidelines. *Agronomy Journal*, 95, 455–471. <https://doi.org/10.2134/agronj2003.4550>

- Corwin, D. L., & Lesch, S. M. (2005). Apparent soil electrical conductivity measurements in agriculture. *Computers and Electronics in Agriculture*, *46*, 11–43. <https://doi.org/10.1016/j.compag.2004.10.005>
- Farahani, H. J., Buchleiter, G. W., & Brodahl, M. K. (2005). Characterization of apparent soil electrical conductivity variability in irrigated sandy and non-saline fields in Colorado. *Transactions of the American Society of Agricultural Engineers*, *48*, 155–168. <https://doi.org/10.13031/2013.17959>
- Garré, S., Coteur, I., Wonglecharoen, C., Kongkaew, T., Diels, J., & Vanderborght, J. (2013). Noninvasive monitoring of soil water dynamics in mixed cropping systems: A case study in Ratchaburi Province, Thailand. *Vadose Zone Journal*, *12*(2). <https://doi.org/10.2136/vzj2012.0129>
- Garré, S., Javaux, M., Vanderborght, J., Pagès, L., & Vereecken, H. (2011). Three-dimensional electrical resistivity tomography to monitor root zone water dynamics. *Vadose Zone Journal*, *10*, 412–424. <https://doi.org/10.2136/vzj2010.0079>
- Huang, J., Purushothaman, R., McBratney, A., & Bramley, H. (2018). Soil water extraction monitored per plot across a field experiment using repeated electromagnetic induction surveys. *Soil Systems*, *2*(1). <https://doi.org/10.3390/soilsystems2010011>
- Jayawickreme, D. H., Van Dam, R. L., & Hyndman, D. W. (2010). Hydrological consequences of land-cover change: Quantifying the influence of plants on soil moisture with time-lapse electrical resistivity. *Geophysics*, *75*, WA43–WA50. <https://doi.org/10.1190/1.3464760>
- King, J. A., Dampney, P. M. R., Lark, R. M., Wheeler, H. C., Bradley, R. I., & Mayr, T. R. (2005). Mapping potential crop management zones within fields: Use of yield-map series and patterns of soil physical properties identified by electromagnetic induction sensing. *Precision Agriculture*, *6*, 167–181. <https://doi.org/10.1007/s11119-005-1033-4>
- Laloy, E., Javaux, M., Vanclooster, M., Roisin, C., & Bièlders, C. L. (2011). Electrical resistivity in a loamy soil: Identification of the appropriate pedo-electrical model. *Vadose Zone Journal*, *10*, 1023–1033. <https://doi.org/10.2136/vzj2010.0095>
- Lavoué, F., Van Der Kruk, J., Rings, J., André, F., Moghadas, D., Huisman, J. A., ... Vereecken, H. (2010). Electromagnetic induction calibration using apparent electrical conductivity modelling based on electrical resistivity tomography. *Near Surface Geophysics*, *8*, 553–561. <https://doi.org/10.3997/1873-0604.2010037>
- Ma, R., McBratney, A., Whelan, B., Minasny, B., & Short, M. (2011). Comparing temperature correction models for soil electrical conductivity measurement. *Precision Agriculture*, *12*, 55–66. <https://doi.org/10.1007/s11119-009-9156-7>
- Martini, E., Werban, U., Zacharias, S., Pohle, M., Dietrich, P., & Wollschläger, U. (2017). Repeated electromagnetic induction measurements for mapping soil moisture at the field scale: Validation with data from a wireless soil moisture monitoring network. *Hydrology and Earth System Sciences*, *21*, 495–513. <https://doi.org/10.5194/hess-21-495-2017>
- Mary, B., Abdulsamad, F., Saracco, G., Peyras, L., Vennetier, M., Mériaux, P., & Camerlynck, C. (2017). Improvement of coarse root detection using time and frequency induced polarization: From laboratory to field experiments. *Plant and Soil*, *417*, 243–259. <https://doi.org/10.1007/s11104-017-3255-4>
- McNeill, J. D. (1980). *Electromagnetic terrain conductivity measurement at low induction numbers*. Mississauga, ON, Canada: Geonics Limited.
- Michot, D., Benderitter, Y., Dorigny, A., Nicoullaud, B., King, D., & Tabbagh, A. (2003). Spatial and temporal monitoring of soil water content with an irrigated corn crop cover using surface electrical resistivity tomography: Soil water study using electrical resistivity. *Water Resources Research*, *39*(5). <https://doi.org/10.1029/2002WR001581>
- Moghadas, D., Jadoon, K. Z., & McCabe, M. F. (2017). Spatiotemporal monitoring of soil water content profiles in an irrigated field using probabilistic inversion of time-lapse EMI data. *Advances in Water Resources*, *110*, 238–248. <https://doi.org/10.1016/j.advwatres.2017.10.019>
- Rhoades, J. D., Raats, P. A. C., & Prather, R. J. (1976). Effects of liquid-phase electrical conductivity, water content, and surface conductivity on bulk soil electrical conductivity. *Soil Science Society of America Journal*, *40*, 651–655. <https://doi.org/10.2136/sssaj1976.03615995004000050017x>
- Robinson, D. A., Abdu, H., Lebron, I., & Jones, S. B. (2012). Imaging of hill-slope soil moisture wetting patterns in a semi-arid oak savanna catchment using time-lapse electromagnetic induction. *Journal of Hydrology*, *416–417*, 39–49. <https://doi.org/10.1016/j.jhydrol.2011.11.034>
- Shanahan, P. W., Binley, A., Whalley, W. R., & Watts, C. W. (2015). The use of electromagnetic induction to monitor changes in soil moisture profiles beneath different wheat genotypes. *Soil Science Society of America Journal*, *79*, 459–466. <https://doi.org/10.2136/sssaj2014.09.0360>
- Srayeddin, I., & Doussan, C. (2009). Estimation of the spatial variability of root water uptake of maize and sorghum at the field scale by electrical resistivity tomography. *Plant and Soil*, *319*, 185–207. <https://doi.org/10.1007/s11104-008-9860-5>
- Stanley, J. N., Lamb, D. W., Falzon, G., & Schneider, D. A. (2014). Apparent electrical conductivity (EC_a) as a surrogate for neutron probe counts to measure soil moisture content in heavy clay soils (Vertosols). *Soil Research*, *52*, 373–378. <https://doi.org/10.1071/SR13142>
- Tsukanov, K., & Schwartz, N. (2020). Relationship between wheat root properties and its electrical signature using the spectral induced polarization method. *Vadose Zone Journal*, *19*(1). <https://doi.org/10.1002/vzj2.20014>
- Viscarra Rossel, R. A., Adamchuk, V. I., Sudduth, K. A., McKenzie, N. J., & Lobsey, C. (2011). Proximal soil sensing: An effective approach for soil measurements in space and time. In D. L. Sparks (Ed.), *Advances in agronomy* (pp. 243–291). London: Academic Press.
- von Hebel, C., Matveeva, M., Verweij, E., Rademske, P., Kaufmann, M. S., Brogi, C., ... van der Kruk, J. (2018). Understanding soil and plant interaction by combining ground-based quantitative electromagnetic induction and airborne hyperspectral data. *Geophysical Research Letters*, *45*, 7571–7579. <https://doi.org/10.1029/2018GL078658>
- von Hebel, C., Rudolph, S., Mester, A., Huisman, J. A., Kumbhar, P., Vereecken, H., & van der Kruk, J. (2014). Three-dimensional imaging of subsurface structural patterns using quantitative large-scale multiconfiguration electromagnetic induction data. *Water Resources Research*, *50*, 2732–2748. <https://doi.org/10.1002/2013WR014864>
- Wasson, A. P., Rebetzke, G. J., Kirkegaard, J. A., Christopher, J., Richards, R. A., & Watt, M. (2014). Soil coring at multiple field environments can directly quantify variation in deep root traits to select wheat genotypes for breeding. *Journal of Experimental Botany*, *65*, 6231–6249. <https://doi.org/10.1093/jxb/eru250>

- Wasson, A. P., Richards, R. A., Chatrath, R., Misra, S. C., Prasad, S. V. S., Rebetzke, G. J., ... Watt, M. (2012). Traits and selection strategies to improve root systems and water uptake in water-limited wheat crops. *Journal of Experimental Botany*, *63*, 3485–3498. <https://doi.org/10.1093/jxb/ers111>.
- Waxman, M. H., & Smits, L. J. M. (1968). Electrical conductivities in oil-bearing shaly sands. *Society of Petroleum Engineers Journal*, *8*, 107–122. <https://doi.org/10.2118/1863-A>
- Whalley, W. R., Binley, A., Watts, C. W., Shanahan, P., Dodd, I. C., Ober, E. S., ... Hawkesford, M. J. (2017). Methods to estimate changes in

soil water for phenotyping root activity in the field. *Plant and Soil*, *415*, 407–422. <https://doi.org/10.1007/s11104-016-3161-1>

How to cite this article: Blanchy G, Watts CW, Ashton RW, et al. Accounting for heterogeneity in the θ – σ relationship: Application to wheat phenotyping using EMI. *Vadose Zone J.* 2020;19:e20037. <https://doi.org/10.1002/vzj2.20037>